Environmental Management (2025) 75:2425–2436
https://doi.org/10.1007/s00267-025-02158-6

Photocatalytic Performance of Ag/Humic Acid Magnetic Nanoparticles for Degradation of Methylene Blue in Aqueous Medium

Ibrahim Kaba[1] · Fatos Ayca Ozdemir Olgun[2]

Received: 16 January 2025 / Accepted: 25 March 2025 / Published online: 9 April 2025

Abstract

The contamination of water as a result of the discharge of organic dyes from industrial facilities that process pharmaceuticals, textile fabrics, leather, and petrochemicals, is a significant concern. The water quality of the aquatic environment is mostly impacted by pigments, even in small amounts less than 1 mgL^{-1} (Sharma et al. 2021). Methylene blue which is considered as mutagenic, toxic, and non-biodegradable, was selected as a model in this study to represent the azo-dye class. The undesired effects of dye contamination can be eliminated through the sustainable and eco-friendly remediation procedure of photocatalytic degradation. The properties and efficiency of the catalytic reaction are significantly influenced by the morphology of the catalyst. Mott Schottky measurements and chronoamperometry were employed to elucidate the electronic properties of a composite silver humic acid magnetic nanoparticle (Ag/HA MNP) with a core-shell structure. The nanoparticle was subsequently employed in the photocatalytic degradation of methylene blue. The indirect band gap energy was calculated as 1.82 eV by employing Ultraviolet-Visible Diffuse Reflectance Spectroscopy (UV-DRS). The optimal parameters established in the study were used to maintain the effective photocatalytic degradation of methylene blue in an aqueous medium. Optimization studies for photocatalytic degradation of model dye-MB showed that the optimum degradation percentage (42%) was achieved rapidly in a short time period of 30 min with 0.06 g MNP in 10 mgL^{-1} solution. The first-order rate constant was determined to be $4.4 \times 10^{-2} s^{-1}$. This study contributes to the literature by proposing Ag/HA magnetic nanoparticles which were synthesized and installed for the first time as a catalyst for the photodegradation of methylene blue in aqueous medium.

Keywords Photocatalytic activity · Remediation · Magnetic nanoparticles · Degradation

Introduction

The most important environmental problems are wastewaters originated from industrial plants and laboratories. Dye compounds are the major components of the discharged wastes that severely effect the health of human beings, aquatic life and microorganisms, leaving deep impacts on the earth's ecosystem (Akpan and Hameed 2009). As it was previously reported in conducted literature, industrial dyes (mainly textile) constitute one of the major groups of organic compounds leading environmental pollution (Tkaczyk et al. 2020). The uncontrolled release of these colored wastewaters is a great concern in terms of non-esthetic pollution, eutrophication and perturbations in the aquatic life (Houas et al. 2001). Since each country defines their own limitations, there is neither common standard level of discharged water quality, nor a specific method to remove the undesired color of wastewaters (Solayman et al. 2023). There are numerous physical, physicochemical, chemical and biological treatment methods introduced including adsorption (Fayazi et al. 2015; Velusamy et al. 2021), membrane filtration (Lim et al. 2021; Gunawan et al. 2018), advanced oxidation processes (Ismail and Sakai 2021), and photocatalytic processes (Ancy et al.

✉ Fatos Ayca Ozdemir Olgun
fatos.olgun@istun.edu.tr

[1] Faculty of Engineering, Department of Chemical Engineering, Marmara University, Maltepe, Istanbul, Turkey

[2] Faculty of Engineering and Natural Sciences, Department of Chemical Engineering, Istanbul Health and Technology University, Sutluce, Istanbul, Turkey

2021; Adekunle et al. 2021; Shan et al. 2020). Advanced oxidative processes (AOPs), including heterogeneous photocatalysis, are effective techniques for treating dye involving waste waters. These processes produce highly oxidizing radicals under UV or visible radiation, mineralizing persistent organic pollutants. To increase photocatalytic efficiency, photocatalysts can be modified with metals, facilitating photoelectrons transfer and reducing band gap energy (Figueiredo et al. 2020; Muraro et al. 2023; Ribas et al. 2020). Photocatalytic treatment is one of the most feasible methods as it is cost-effective, environmentally friendly, yielding high removal rate within short duration and worldwide popularity. Nanotechnology is revolutionizing the synthesis of new nanostructured systems, including magnetic nanoparticles (MNPs), with high surface area potential for heterogeneous photocatalysis applications (De Menezes et al. 2023). Magnetite (Fe_3O_4) nanoparticles (NPs), whose morphology and composition play an important role in magnetic response (Özkul et al. 2024), are frequently suggested as ideal core materials due to their low toxicity, biocompatibility (Rosman et al. 2018), high magnetization, superior photon absorption ability, and dipole-dipole interactions that enable strong bonds (Yang et al. 2009) according to recent studies in the field of photocatalysis. Besides, as their application is through the magnetic field, the mobility of Fe_3O_4 NPs is easy to operate within the degradation process.

One of the major drawbacks for the application of ferrite nanoparticles is their low separation efficiency of electrons and holes (Cao et al. 2007), which leads to a much lower photocatalytic activity. It has been shown that the deposition of a noble metal at nanoparticle surface increases the separation rate of electrons by directing the flow of the photogenerated charges towards the opposite directions (He et al. 2002). Therefore, silver was coated to enhance both the formation of reactive species and the photocatalytic activity by recombination of the generated electron/hole pairs. Noble metals like Ag, Au, and Pt nanoparticles have been used as cocatalysts to enhance catalytic performance in various fields. The Surface Plasmon Resonance (SPR) effect promotes visible light absorption due to the well-aligned interface between semiconductor and noble metals. Metallic silver (Ag°) is a popular cocatalyst due to its low cost, excellent activity, unique electrical conductivity, and high stability. It also acts as an electron mediator in Z-scheme plasmonic photocatalysts, enhancing visible light response (Padervand et al. 2020; Heidarpour et al. 2020; Padervand et al. 2022a). For example, $ZnTiO_3$-based plasmonic structures were investigated for photocatalytic treatment of glioblastoma tumor cells under visible irradiation (Padervand et al. 2022b).

Humic acid (HA) is a heterogenous mixture of polycationic and anionic materials that is an important fraction of natural organic matter (NOM). A thin layer of HA coating on the outer surface of magnetic nanoparticles (Fe_3O_4) inhibits the oxidation and agglomeration of magnetic nanoparticles (MNP)s by protecting the Fe_3O_4 core (Pham et al. 2020). Since there are various studies to investigate the adsorptive behavior of HA coated MNPs, their photocatalytic properties to treat aquatic systems have not been enlightened particularly (Zhang et al. 2023; Xue et al. 2023). A few studies involving HA influence on nanoparticles and the interaction between metal nanoparticles with surrounding molecules in aqueous environment were previously reported (Li and Hu 2016). Wu et al. presented the promotive effect of HA concentration on the photodegradation of bisphenol A by nano-TiO_2 (Wu et al. 2016). Therefore, making use of its features discussed above, HA carries potential and worth to be proposed as a sustainable, abundant, non hazardous raw material for the modification of nanomaterials.

This study aims to investigate the utilization of Ag and humic acid coated Fe_3O_4 magnetic nanoparticles (Ag/HA MNPs) that were fabricated according to the previously optimized procedure (Mashhadizadeh 2012). It holds significance as it is the first study in literature, proposing the installation of a novel material (Ag/ HA MNPs) as a catalyst for the degradation process of methylene blue in waste waters.

Materials and Methods

Reagents

Ammonium iron(II)sulfate hexa hydrate, humic acid sodium salt, ammonia solution (25%), tin(II)chloride, methylene blue, ethylene glycol, hydrochloric acid and sodium hydroxide were purchased from Merck, Germany. Ferrous chloride hexa hydrate (Fluka, 98% pure) was used for magnetic nanoparticle synthesis. Distilled water was employed during all experiments. All the chemicals used during the experiments were of analytical grade.

In order to create a real-world scenario, real waste-water sample was obtained from a leather processing company in Gebze Organized Leather Industry Region, Istanbul, Turkey. The exact chemical composition of the wastewater is patented to the company, whereas cationic dye content was declared by the authorities.

Instrumentation

A Chiltelrn Hotplate Magnetic Stirrer was used to achieve homogeneous heating during the co-precipitation process of nanoparticles. A regular magnet was used to collect particles from the sample solution. For successful coating at all

stages of synthesis BANDELIN RK100H ultrasonic bath was used. MNPs are analyzed using a UV–vis diffuse reflectance spectrometer (PG Instruments T92^{+} UV/VIS) for determining the band gap energies. A HAL-320 Compact Xenon Light Source Solar Simulator served as the lights source, and light intensity was measured using a light meter (HD 2302.0). The light intensity was concentrated to one-sun (1000 Wm^{-2}). All photoelectrochemical measurements were conducted utilizing a potentiostat/galvanostat (Gamry Interface 1000) together with software (Gamry Framework and Gamry Echem Analyst). A Bruker D2 Phaser X-Ray diffractometer (Cu-Kα radiation (1.54185 A), 30 kV voltage and 10 mA^{0} current) was used to perform X-Ray Diffraction (XRD) analyses for MNPs before and after the degradation process, to observe the effect of recycle on the surface characteristics.

Synthesis of Ag/ HA MNPs

One of the easiest and most practical methods for the synthesis of Fe_3O_4 NPs is chemical co-precipitation iron chloride salts in alkaline medium (Mashhadizadeh 2012). Similar synthesis procedure proposed by Olgun et al. was installed for the synthesis of Ag/HA MNPs. Accordingly, $FeCl_3.6H_2O$, $NH_4FeSO_4.6H_2O$ and Fe_3O_4 mixture was heated to 90 °C. At this temperature, 1.0 mg L^{-1} humic acid sodium salt solution was added with iron (III) chloride and iron(II) chloride solutions. Subsequently, 25% ammonia solution addition allowed the precipitation of HA coated magnetite nanoparticles (Olgun et al. 2018). HA coating helped to form a site for Ag settling through a thin a layer of Sn^{2+} that was absorbed earlier onto the shell of Ag/HA MNPs by electrostatic attraction. With the aid of this thin layer, silver coating of the particles occured with the aid of redox reaction taking place between Sn^{2+} ions and Ag^{+} ions (Wang et al. 2016). The final multicomponent structure (Ag/HA MNPs) was separated from the original suspension with the aid of a simple magnet and allowed to dry at 60 °C.

Optical Characterization of MNPs

The morphological studies of the magnetic nanoparticles were previously investigated by conducted literature (Mashhadizadeh 2012). The electronic properties were evaluated by Mott Schottky measurements. In optical studies, indirect band-gap energies were calculated with the aid of Ultraviolet-Visible Diffuse Reflectance Spectroscopy (UV-vis DRS).

Since ITO glass is not conductive, the conductivity was measured with a voltmeter, following the conductivity measurement, the conductive part was closed. Efficient amount of sample and ethylene glycol were mixed and coated on ITO glass with the aid of DR blade. The samples were then dried at 50 °C in magnetic active and calcined at 200 °C. Current density and Mott-Schottky plots were performed in a standard three-electrode cell, using ITO glass (20 mm × 20 mm) loaded with a modest quantity of photocatalyst as the working electrode, a Pt plate as the counter electrode, and an Ag/AgCl electrode as the reference electrode. The electrolyte utilized was a 0.5 M aqueous Na_2SO_4 solution. A solar simulator was employed as it simulated the sun source for photocurrent responses, with a light-shift time of 50 s from on to off. A three-electrode device was utilized to measure Mott-Schottky curves (MS) at 500 Hz.

Photocatalytic Degradation of Methylene Blue

The photocatalytic properties of magnetic nanoparticles were examined with methylene blue solution that was utilized as the target organic dye. The prepared sample and dye mixture were placed under a solar simulator and stirred continuously. 10 mgL^{-1} MB solution was prepared and 0.06 g of photocatalyst (HA/Ag MNPs) was added to 80 mL MB solution. The solutions were then allowed to stand in the dark for an hour to sustain the adsorption-desorption mechanism. The amount of absorbed dye can be calculated by comparing the dye concentrations before and after the dark response. After one hour, a portion of 5 mL was decantated from the solution and suspended photocatalyst particles were separated from the aliquot with aid of a simple magnet. The absorbance values of the supernatant were measured at 665 nm using a UV-Visible spectrophotometer. Similar experiments were performed at varying dosage and initial MB concentration values for the optimization of photocatalytic degradation process. All catalytic experiments were carried in triplicates so as to ensure the accuracy and consistence of the results.

The percentage of MB degradation (D%) was expressed in accordance with the following expression:

$$D\% = \frac{C}{C_0} \tag{1}$$

Where, C is the concentration of MB at final solution and C_0 is the initial concentration of MB at t = 0.

The evaluation of reaction kinetics carries major importance for the determination of reaction rate constant and half-time. In order to simplify heterogeneous catalytic processes, pseudo-first-order kinetics model may be installed, and further expressions were used to calculate the parameters which are defined within the model.

$$ln\frac{C0}{C} = kt \tag{2}$$

$$t_{1/2} = \frac{ln2}{k} \tag{3}$$

Application of the Method to Industrial Wastewaters

The optimal conditions of photocatalytic degradation of predetermined for methylene blue model dye were applied to real wastewaters of a leather dyeing plant. The wastewaters were supplied from a leather processing factory in Leather Organized Industry Zone, Tuzla. As the dye content of the sample was unknown due to commercial confidentiality, the samples were spiked with 10 mgL^{-1} MB solution. Methylene blue degradation percentage values were calculated using absorbance values at 665 nm according to Eqs. (1) and (2).

Recycle of the Photocatalyst

Due to their magnetic properties, magnetic nanoparticles are considered as enviromental friendly, cost effective and easy-to-operate materials that may be suggested for photocatalytic processes. The recyclability of these photocatalysts is one of the key points to determine their reusability and long-term photocatalytic activity. Therefore, Ag/HA MNPs were discarded from the supernatant at the end of the first degradation process with a simple magnet, washed with deionized water without utilizing an additional regeneration step and dried at 60 °C. The recovered particles were used in accordance with the same photocatalytic procedure described in Section 2.4. To observe the regeneration of MNPs, degradation of real sample was studied as three cycles for 30 min.

Results and Discussions

The powder XRD pattern of MNPs is depicted in Fig. 1a. The prominent primary Bragg reflections at 2θ of 30.29∘, 35.60∘, 43.33∘, 53.64∘, 57.33∘, and 62.98∘ can be indexed to the (220), (311), (400), (422), (511), and (440) planes, respectively, by comparison with JCPDS card No. 00-019-0629 (Yadav et al. 2020). The detailed and sharp diffraction peaks indicate that the product has high purity and good crystalline particle structure (Mohan et al. 2022a).

Figure 1b indicates that the FTIR spectrum has a peak at 548.12 cm^{-1}, which corresponds to the oxygen-metal (Fe-O) vibration in iron oxide nanostructures, and another peak at 1622.98 cm^{-1}, which corresponds to the C = O bond (Sihem et al. 2020). The presence of alkoxy C–O stretching vibrations (1106 cm^{-1}) and carboxyl O = C–O (1415 cm^{-1}) was proven (Khoshnam et al. 2021). The peak at 3451 cm^{-1} was assigned to the OH stretching vibration of adsorbed water (Qin et al. 2010). Furthermore, as silver does not absorb electromagnetic radiation in the infrared region of the spectrum, was not observed within the graph (Sallam et al. 2018).

XPS analyses were performed to further characterize the surface chemical composition of Ag/HA MNPs. Figure 1c shows a typical XPS scanning spectrum for Ag/HA MNPs. The XPS profile shows that Fe 2p, O 1 s, and C 1 s peaks were observed in the hybrids, suggesting that the sample mainly contains three elements, Fe, O, and C. Silver was suppressed in the XPS analysis as in other characterization methods and showed a similar peak at around 375 eV as in previous studies (Han et al. 2019; Kumar et al. 2024).

Optical Characterization Studies

Figure 2 displays the UV–visible-DRS spectrum and Tauc plot of the prepared Ag/HA MNPs. As it is shown by the graph, the material absorbs electromagnetic radiation in visible regions of the spectrum, suggesting a photocatalytic activity, especially under solar light (Fig. 2a). Tauc method that assumes that the energy-dependent absorption coefficient (α) which relies upon the energy of photon hυ, is utilized to estimate the bandgap energy (E_g). Tauc Plot was constructed as $(\alpha h\nu)^{1/2}$ vs $h\nu$ to calculate the indirect band gap energy of the material and is displayed by Fig. 2b. The indirect band gap energy of the material was calculated as 1.82 eV, with the aid of the Tauc plot (Fig. 2b), in accordance with Tauc Equation given by the following expression:

$$(\alpha h\nu)^n = A(h\nu - Eg) \quad (4)$$

In the given expression, A is the proportionality constant, α is the coefficient of absorption and the exponent n is a function of the nature of the transition (1/2 for indirect transitions). In the calculation, the Kubelka-Munk function was used for band gap analysis and $n = 1/2$ (indirect band gap) was applied to MNPs (Bozkurt and Şahin 2024).

Photoelectrochemical evaluation of MNPs

Photocurrent measurements of MNPs were evaluated by the broadband spectrum responsiveness performance. After the modification of ITO substrates with Ag/ HA MNPs, a response photocurrent with repeatable on/off cycles upon light irradiation was observed. The sharp density curves in Fig. 3a displays the photocurrent density curves under chopper light illumination.

The dramatic increase and decrease in photocurrent density were recorded due to the on/off position of the irradiation. It may be observed from the figure that the photocurrent density (chronoamperometry) is steady and reproducible during several intermittent on–off irradiation cycles, for 600 s as 100 s time intervals. There is a strong relationship between the photocurrent and effective charge separation and transport over the surface of a photocatalyst

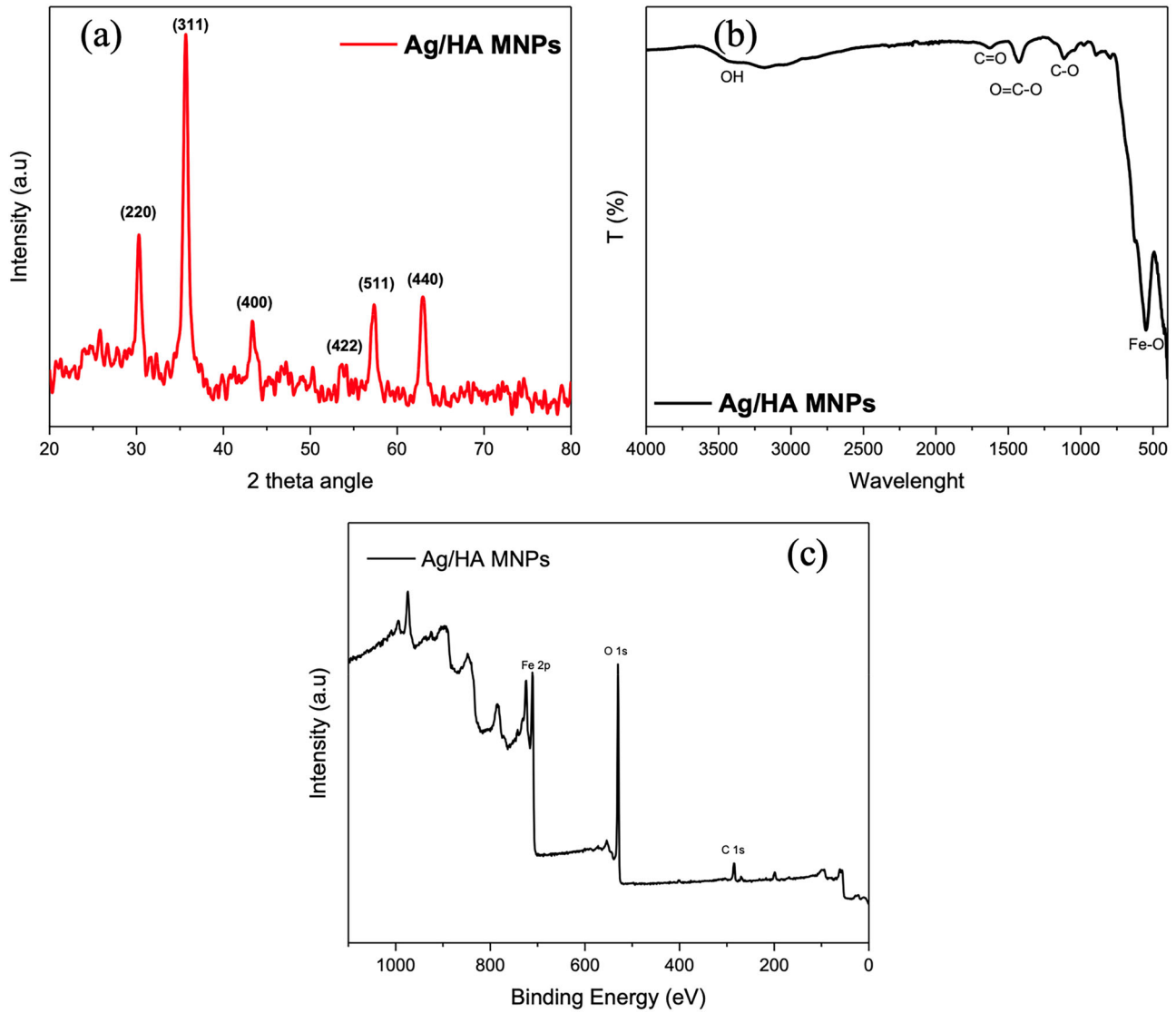

Fig. 1 **a** XRD patterns of Ag/HA MNPs, (**b**) FTIR spectra of Ag/HA MNPs, (**c**) survey XPS spectrum of Ag/HA MNPs

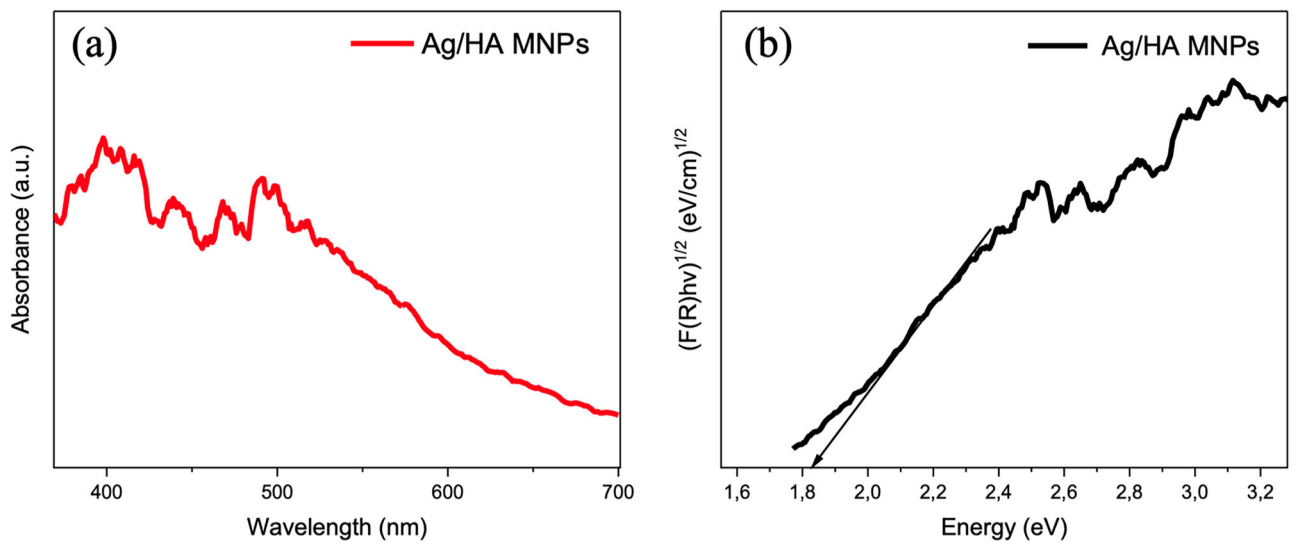

Fig. 2 **a** UV-DRS Spectrum of Ag/ HA MNPs, (**b**) Tauc Plot OF UV-DRS spectrum of Ag/ HA MNPs

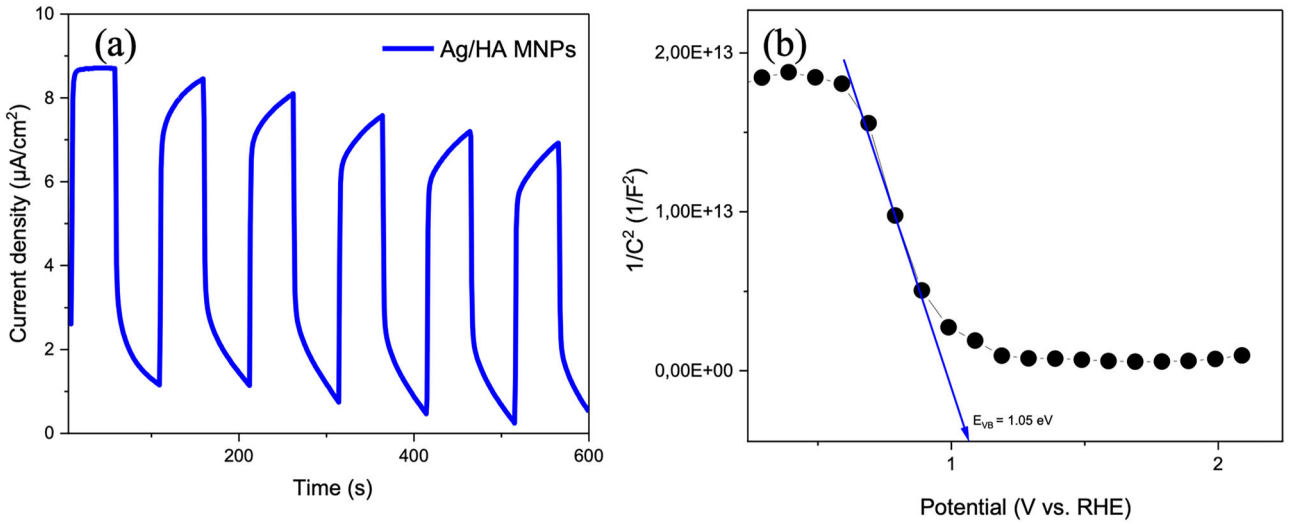

Fig. 3 **a** Photocurrent density of Ag/HA MNPs, (**b**) Mott-Schottky Plot of Ag/ HA MNPs

(Wang et al. 2020). It may be resulted that the photocurrent density of the MNPs favors the separation and transfer efficiency of photogenerated electron–hole pairs to the surface where photocatalytic reaction occurs.

The Mott-Schottky curve depicts the flat band potential at the interface of the semiconductor and the liquid. The flat band potential can be calculated from the graph using the equation illustrated by Eq. (5) where N is density of the charge carrier, C is the capacitance of the space-charge region, q_e is electronic charge, V is applied potential; T is Absolute temperature, $\in_o$= free space permittivity, K is Boltzmann constant and $\in$ is the dielectric constant of the semi-conductor and E_{fb} is flat band gap potential (Nasir et al. 2020).

$$\frac{1}{C^2} = \frac{2}{N \in \in_0 e}\left(E - E_{fb} - \frac{KT}{q_e}\right) \quad (5)$$

As shown in Fig. 3, the slope of Mott-Schottky curve has a negative slope, which fits the characteristics of a p-type semiconductor (Xu et al. 2022). The flat band potential (E_{fb}) values of the nanoparticles were found by extrapolating the linear region of the plot to the intercept of the x-axis. The calculated flat band potentials (E_{fb}) for the sample were 1.05 V with respect to the normal hydrogen electrode (NHE) (Velegraki et al. 2019).

The n-type and p-type semiconductors are denoted by the positive and negative slopes, respectively. Furthermore, the Mott-Schottky plot can be extrapolated to estimate the flat band potential (E_{fb}) of the semiconductor, which can be used to determine the location of the Fermi level. The extrapolated flat band potential (E_{fb}) can be employed to determine the location of the edge of the n-type semiconductor (E_{CB}) or p-type semiconductor (E_{VB}) if the Fermi level is in close proximity to the band edge (Shan et al. 2023). Consequently, the equation below can be employed to determine the E_{VB} of Ag/HA MNPs:

$$E_{VB} = E_g + E_{CB} \quad (6)$$

where E_g denotes the energy of the optical band gap (Kaba and Kerkez-Kuyumcu 2024). The Mott-Schottky diagrams of MNPs are depicted in Fig. 3b with Ag/AgCl serving as the reference electrode. When the difference between the reference electrode (Ag/AgCl) and the standard value of 0.19 eV is added to the value of 1.05 eV obtained from the Mott-Schottky diagram, the estimated E_{VB} value for Ag/HA MNPs is 1.24 eV. When E_{CB} is calculated using Eq. (6), if the approximately 1.82 eV band gap found in Fig. 2b is subtracted from the calculated 1.24 eV (E_{VB}), E_{CB} is calculated as approximately −0.58 eV (Zhang et al. 2021). The possible mechanism for MNPs used in the photocatalytic degradation system for the obtained values is shown in Fig. 4.

Photodegradation of Methylene Blue

Optimization Studies

Ag/HA MNPs are proposed as heterogenous photocatalysts for the photodegradation studies of MB in wastewaters. For this purpose, parameters such as duration and dose of catalyst were optimized in order to enhance the efficiency of photocatalytic degradation.

Determination of the accurate dose of photocatalyst to be used in the photodegradation process is one of the major effects that should be evaluated for economic purposes (Amoli-Diva et al. 2019). It is usually assumed that the catalyst dosage is directly proportional to the degradation percentage; however, the influence of increasing turbidity of the catalyst and dye solution mixture on the length of penetrating electromagnetic radiation should not be

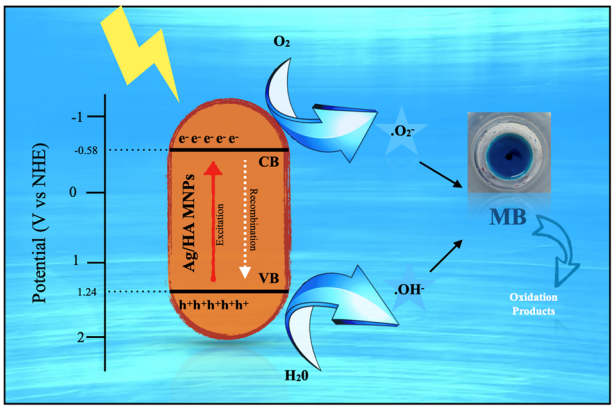

Fig. 4 Schematic illustration of the possible photocatalytic reaction mechanism of Ag/HA MNPs

underestimated. Figure 5a depicts the effect of catalyst by displaying the photodegradation of MB at absence of Ag/HA MNPs. The catalyst at varying amounts between 0.03 g and 0.12 g was weighed and mixed with MB solution as described in the experimental procedure. Figure 5b–d shows the effect of catalyst dose on the photocatalytic degradation of MB in aqueous medium. Figure 5e, f shows that after optimization of the catalyst dose, the initial concentrations of the target dye were varied between 5 mg L^{-1} and 20 mg L^{-1} to evaluate the correct catalyst dose (0.06 g). As a result, installing the optimized parameters, the photocatalytic degradation of MB by the fabricated photocatalyst Ag/HA MNPs was performed under the light source of solar simulator for 30 min. Prior to the reaction under visible light, adsorption–desorption equilibrium was established in dark for 1 h.

Mechanism and Kinetic Studies of Photodegradation

It is considered that the degradation of MB in aqueous medium is initiated by photoexcitation of the nano catalyst and followed by the formation of e^-/h^+ pairs on the surface. The suggestion of mechanism for the degradation of MB is given by the following equations (Eqs. 7)–(12).

$$Photocatalyst + h\nu \rightarrow e^-_{CB} + h^+_{vb} \quad (7)$$

$$h^+_{vb} + MB \rightarrow Oxidation\ products \quad (8)$$

$$e^-_{CB} + O_2 \rightarrow \cdot O_2^{-*} \quad (9)$$

$$h^+_{vb} + H_2O \rightarrow H^+ + OH^- \quad (10)$$

$$h^+_{vb} + \cdot OH^- \rightarrow OH^* \quad (11)$$

$$MB + OH^* + O_2^{-*} \rightarrow Oxidation\ Products \quad (12)$$

Surface reactions with holes generate in the valence band (VB) causing a transformation of hydroxyl radicals while the dissolved oxygen reacts with electrons of the conduction band (CB) producing superoxide radicals (Mohan et al. 2022b). It may be proposed that the holes oxidize the organic compounds, and the electron-hole pair recombination is disabled by the electrons captured by the catalyst surface.

Determination of the kinetic model is significant to enlighten the photocatalytic degradation of MB. The pseudo-first-order model (Eq. (13)) was found to be compatible with the present degradation kinetics, confirmed by the graph displayed in Fig. 6a ($R^2 = 0.98$).

$$ln\frac{C}{C_0} = -k't \quad (13)$$

In the given expression, C and C_0 are the concentrations (mg L^{-1}) of MB at time, t and t = 0, where k' is the pseudo-first-order rate constant expressed in sec^{-1} and determined from the slope of the curve drawn as ln C/C_0 versus time (Benrighi et al. 2021). The first-order rate constant was calculated to be $4.4 \times 10^{-2}\,s^{-1}$. It was previously reported that the photocatalytic degradation of organic pollutants is recognized by their correlation with pseudo-first-order kinetics (An et al. 2002), that is also supported by the findings of the present study.

Photodegradation of Industrial Wastewater

Optimized conditions for the photocatalytic degradation of MB in presence of Ag/HA MNPs were applied to real samples in order to test the applicability of the proposed catalyst in complicated sample matrix. As it is displayed in Fig. 6b, the dramatic decrease at the absorbance values after 30 min, supports the utilization of MNPs in real sample medium.

The recyclability of the catalyst is another important issue to evaluate in case of eco-friendly approaches. For the investigation of reusability, Ag/HA MNPs were first separated from the initial sample after photocatalytic degradation with the aid of their magnetic properties and washed with deionized water without utilizing an additional regeneration step and dried at 60 °C. The regenerated particles were reused for the degradation of a freshly prepared sample solution. The degradation percentages stayed constant even after 3 cycles (Fig. 6c) confirming the stability and efficacy of recovered photocatalysts for the degradation of wastewater samples. Additionally, XRD spectra of the original and regenerated MNPs (Fig. 6d) were compared to observe the changes at their structure after recycle process and found to be similar in terms of peak identification. For the evaluation of the findings, Table 1 is introduced as a summary of recent studies on photocatalytic degradation of MB.

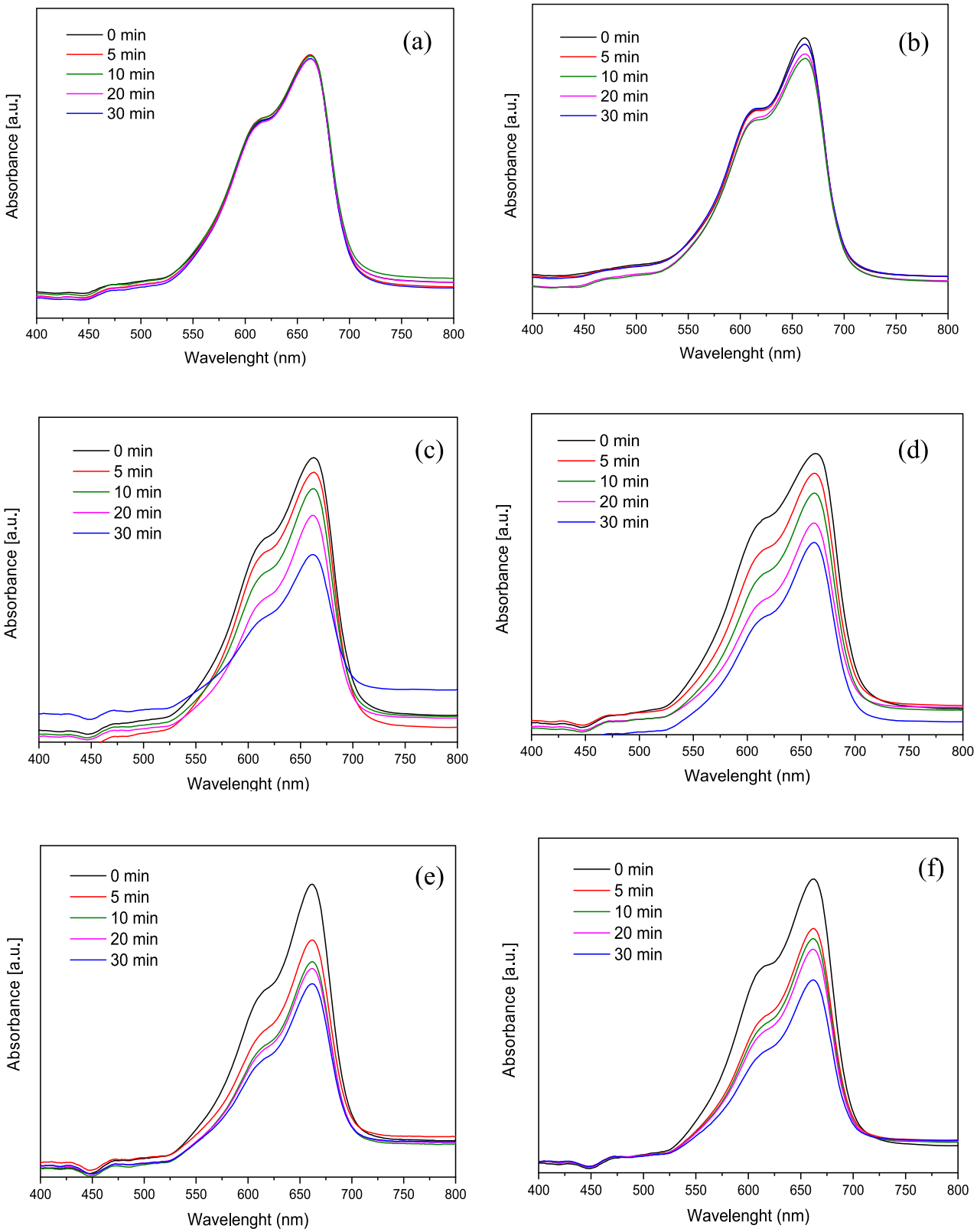

Fig. 5 **a** Photodegradation of 10 mgL^{-1} MB at varying time intervals. Photocatalytic degradation of 10 mgL^{-1} MB at varying time intervals in the presence of Ag/HA MNPs using (**b**) 0.03 g, (**c**) 0.06 g, and (**d**) 0.12 g MNPs. Photocatalytic degradation of (**e**) 5 mgL^{-1} and (**f**) 20 mgL^{-1} MB at varying time intervals in the presence of Ag/HA MNPs using 0.06 g MNPs

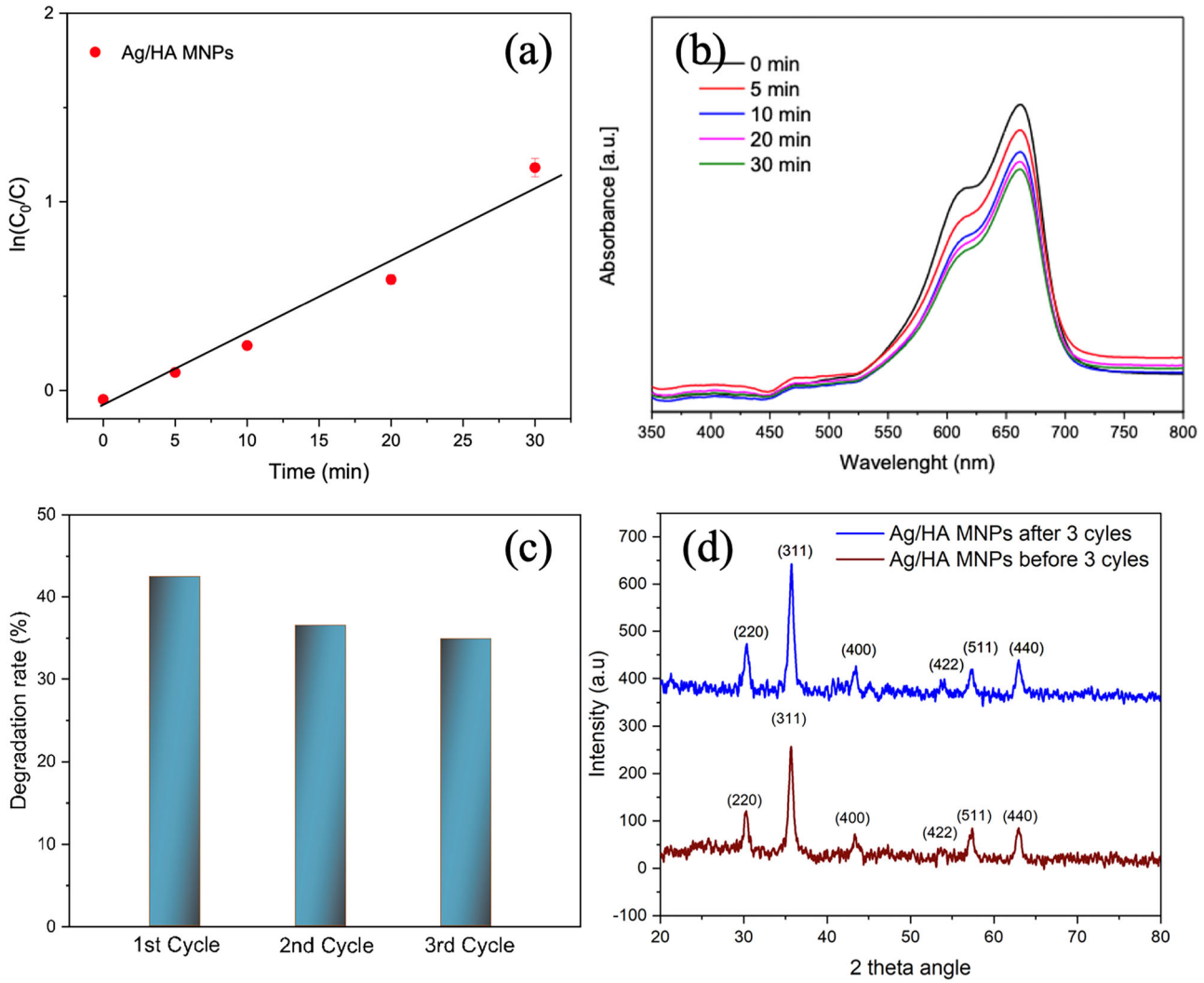

Fig. 6 **a** Photocatalytic degradation kinetics for MB, (**b**) the UV–Vis spectra of initial leather waste water before and after photocatalytic degredation at varying time intervals, (**c**) recyclability test for Ag/HA MNPs for 3 cycles (**d**) XRD spectra of Ag/HA MNPs before and after the treatment of real samples

Table 1 Some recent studies on photocatalytic degradation of MB, conducted in the literature

Type of Catalyst	Degradation % of MB	Duration (min)	Reference
TiO_2 NP	88.51	120	Niu et al. (2021)
TiO_2 NP	40.0	300	Nasikhudin et al. (2020)
$Mg_{(0.6)}Zn_{(0.4)}Fe_2O_4$ MNPs	16.67	35	Alzahrani et al. (2024)
$CuxMg_{(0.6)}Zn_{(0.4)}Fe_2O_4$ MNPs	42.72	35	Alzahrani et al. (2024)
Fe_2O_3/TiO_2 nanoparticles	30.0	60	Ahmed et al. (2012)
HA/ ZnO nanoparticle	50.0*	60	Chandran et al. (2014)
Ag/HA MNPs	42.0	30	This study

(* varies with the concentration of HA)

Conclusion

In this study, Ag/HA MNPs (with a mean diameter of 291 nm) were synthesized following 2 steps as coprecipitation and electroplating. The flat band energy was estimated as −1.05 with the aid of Mott-Schottky Method and indirect band gap energy was found as 1.82 eV which allows the fabricated Ag/HA MNPs to be used as photocatalyst. In accordance with the reaction mechanism, it may be suggested that the holes oxidize the organic compounds, and electrons captured by the catalyst surface prevents the recombination electron hole pairs. Optimization studies for

the photocatalytic degradation of the model dye-MB showed that the maximum degradation percentage (42%) is obtained with 0.06 g of MNPs within a short time period (30 min). Fabricated photocatalysts may be used recycling 3 times and do not require additional regeneration procedure. The kinetics of MB degradation was evaluated measuring the rate constant and found compatible with Pseudo First Order kinetics. Furthermore, the magnetic core promotes the recovery of photocatalysts by applying an external magnetic field, supporting MNPs to display enhanced recycling properties, using deionized water for regeneration. The research work also holds significance by following the advantage of an abundant organic matter, HA and proposing it as a sustainable raw material for the modification of photocatalysts (Tan et al. 2024). It is well known that the toxicologic effects of nanoparticles in aquatic media decrease through the coating of HA (Chandran et al. 2014), still further studies are required for the evaluation of their toxicologic effects. In conclusion, HA coated MNPs are promising for the photodegradation of organic pollutants by heterogeneous photocatalysis and are potentially applicable in real samples.

Data availability

No datasets were generated or analysed during the current study.

Author contributions All authors whose names appear on the submission made substantial contributions to the conception or design of the work and contributed equally. FAO Olgun acts on behalf of the co-author, as the corresponding author.

Compliance with ethical standards

Conflict of interest The authors declare no competing interests.

References

Adekunle AS, Oyekunle JAO, Durosinmi LM et al. (2021) Comparative photocatalytic degradation of dyes in wastewater using solar enhanced iron oxide (Fe2O3) nanocatalysts prepared by chemical and microwave methods. Nano-Struct Nano-Objects 28:100804. https://doi.org/10.1016/j.nanoso.2021.100804.

Ahmed MA, El-Katori EE, Gharni ZH (2012) Photocatalytic degradation of methylene blue dye using Fe2O3/TiO2 nanoparticles prepared by sol–gel method. J Alloy Compd 553:19–29. https://doi.org/10.1016/j.jallcom.2012.10.038.

Akpan UG, Hameed BH (2009) Parameters affecting the photocatalytic degradation of dyes using TiO2-based photocatalysts: A review. J Hazard Mater 170:520–529. https://doi.org/10.1016/j.jhazmat.2009.05.039.

Alzahrani FMA, Parveen S, Alrowaili ZA et al. (2024) CUXMG(0.6)ZN(0.4)FE2O4 nanomaterials and their composite for photocatalytic degradation of colored and colorless effluents under xenon lamp. Journal of Inorganic and Organometallic Polymers and Materials. https://doi.org/10.1007/s10904-024-03040-4

Amoli-Diva M, Anvari A, Sadighi-Bonabi R (2019) Synthesis of magneto-plasmonic Au-Ag NPs-decorated TiO2-modified Fe3O4 nanocomposite with enhanced laser/solar-driven photocatalytic activity for degradation of dye pollutant in textile wastewater. Ceram Int 45:17837–17846. https://doi.org/10.1016/j.ceramint.2019.05.355.

An T-C, Zhu X-H, Xiong Y (2002) Feasibility study of photoelectrochemical degradation of methylene blue with three-dimensional electrode-photocatalytic reactor. Chemosphere 46:897–903. https://doi.org/10.1016/s0045-6535(01)00157-6.

Ancy K, Bindhu MR, Bai JS et al. (2021) Photocatalytic degradation of organic synthetic dyes and textile dyeing waste water by Al and F co-doped TiO2 nanoparticles. Environ Res 206:112492. https://doi.org/10.1016/j.envres.2021.112492.

Benrighi Y, Nasrallah N, Chaabane T et al. (2021) Photocatalytic performances of ZnCr2O4 nanoparticles for cephalosporins removal: Structural, optical and electrochemical properties. Opt Mater 115:111035. https://doi.org/10.1016/j.optmat.2021.111035.

Bozkurt RNN, Şahin S (2024) Green synthesis of zinc oxide nanoparticles including Rosehip (Rosa canina L.) seed extract: Evaluation of its characterization and bioactivity properties. Chem Biodiversity. https://doi.org/10.1002/cbdv.202402724.

Cao X, Gu L, Lan X et al. (2007) Spinel ZnFe2O4 nanoplates embedded with Ag clusters: Preparation, characterization, and photocatalytic application. Mater Chem Phys 106:175–180. https://doi.org/10.1016/j.matchemphys.2007.05.033.

Chandran P, Netha S, Khan SS (2014) Effect of humic acid on photocatalytic activity of ZnO nanoparticles. J Photochem Photobio B Biol 138:155–159. https://doi.org/10.1016/j.jphotobiol.2014.05.013.

De Menezes LB, Muraro PCL, Druzian DM et al. (2023) Calcium oxide nanoparticles: Biosynthesis, characterization and photocatalytic activity for application in yellow tartrazine dye removal. J Photochem Photobio a Chem 447:115182. https://doi.org/10.1016/j.jphotochem.2023.115182.

Fayazi M, Afzali D, Taher MA et al. (2015) Removal of Safranin dye from aqueous solution using magnetic mesoporous clay: Optimization study. J Mol Liq 212:675–685. https://doi.org/10.1016/j.molliq.2015.09.045.

Figueiredo VM, Lourenço JB, De Vasconcellos NJS, Da Silva WL (2020) Preparation, characterization and photocatalytic activity of activated charcoal from microalgae for photocatalytic degradation of rhodamine B dye. Cerâmica 66:367–372. https://doi.org/10.1590/0366-69132020663802937.

Gunawan FM, Mangindaan D, Khoiruddin K, Wenten IG (2018) Nanofiltration membrane cross-linked by m-phenylenediamine for dye removal from textile wastewater. Polym Adv Technol 30:360–367. https://doi.org/10.1002/pat.4473.

Han T, Wei Y, Jin X et al. (2019) Hydrothermal self-assembly of α-Fe2O3 nanorings@graphene aerogel composites for enhanced Li storage performance. J Mater Sci 54:7119–7130. https://doi.org/10.1007/s10853-019-03371-5.

He C, Yu Y, Hu X, Larbot A (2002) Influence of silver doping on the photocatalytic activity of titania films. Appl Surf Sci 200:239–247. https://doi.org/10.1016/s0169-4332(02)00927-3.

Heidarpour H, Golizadeh M, Padervand M et al. (2020) In-situ formation and entrapment of Ag/AgCl photocatalyst inside cross-linked carboxymethyl cellulose beads: A novel photoactive hydrogel for visible-light-induced photocatalysis. J Photochem Photobio a Chem 398:112559. https://doi.org/10.1016/j.jphotochem.2020.112559.

Houas A, Lachheb H, Ksibi M et al. (2001) Photocatalytic degradation pathway of methylene blue in water. Appl Catal B Environ Energy 31:145–157. https://doi.org/10.1016/s0926-3373(00)00276-9.

Ismail GA, Sakai H (2021) Review on effect of different type of dyes on advanced oxidation processes (AOPs) for textile color

removal. Chemosphere 291:132906. https://doi.org/10.1016/j.chemosphere.2021.132906.
Kaba İ, Kerkez-Kuyumcu Ö (2024) Optimization of the boosted photocatalytic H 2 production by rationally designated Cd x Zn 1-x S/MoS 2. Int J Green Energy 1–11. https://doi.org/10.1080/15435075.2024.2397010.
Khoshnam M, Farahbakhsh J, Zargar M et al. (2021) α-Fe2O3/graphene oxide powder and thin film nanocomposites as peculiar photocatalysts for dye removal from wastewater. Sci Rep 11:. https://doi.org/10.1038/s41598-021-99849-x.
Kumar KMA, Kokulnathan T, Wang T-J et al. (2024) Photochemical-assisted deposition of Ag nanoparticles on α-Fe2O3 snowflakes for ultra-sensitive SERS detection of nitrofurazone. Appl Surf Sci 660:160000. https://doi.org/10.1016/j.apsusc.2024.160000.
Li S, Hu J (2016) Photolytic and photocatalytic degradation of tetracycline: Effect of humic acid on degradation kinetics and mechanisms. J Hazard Mater 318:134–144. https://doi.org/10.1016/j.jhazmat.2016.05.100.
Lim YJ, Lee SM, Wang R, Lee J (2021) Emerging materials to prepare mixed matrix membranes for pollutant removal in water. Membranes 11:508. https://doi.org/10.3390/membranes11070508.
Mashhadizadeh MH (2012) Drug-Carrying amino silane coated magnetic nanoparticles as potential vehicles for delivery of antibiotics. J Nanomed Nanotechnol 03: https://doi.org/10.4172/2157-7439.1000139
Mohan H, Sathya PM, Vadivel S et al. (2022) Highly efficient visible light photocatalysis of Ni Zn Fe2O4 (x= 0, 0.3, 0.7) nanoparticles: Diclofenac degradation mechanism and eco-toxicity. Chemosphere 301:134699. https://doi.org/10.1016/j.chemosphere.2022.134699.
Mohan NS, Gokulkumar R, Shankar J et al. (2022) A facile green approach of Fe2O3, Fe2O3 @Ag, Fe2O3 @AC and Fe2O3 @Ag@AC NPs synthesized via Cocos nucifera L for waste water treatment applications. Results Chem 4:100626. https://doi.org/10.1016/j.rechem.2022.100626.
Muraro PCL, Wouters RD, Chuy GP et al. (2023) Titanium dioxide nanoparticles: green synthesis, characterization, and antimicrobial/photocatalytic activity. Biomass- Convers Biorefinery 14:25279–25292. https://doi.org/10.1007/s13399-023-04542-w.
Nasikhudin N, Diantoro M, Kusumaatmaja A, Triyana K (2020) Enhancing photocatalytic performance by sonication and surfactant addition on the synthesis process of PVA/TiO2 nanofibers membranes by electrospinning method. AIP Conf Proc 2251:040045. https://doi.org/10.1063/5.0017654.
Nasir SNS, Mohamed NA, Tukimon MA et al. (2020) Direct extrapolation techniques on the energy band diagram of BiVO4 thin films. Phys B Condens Matter 604:412719. https://doi.org/10.1016/j.physb.2020.412719.
Niu L, Zhao X, Tang Z et al. (2021) Difference in performance and mechanism for methylene blue when TiO2 nanoparticles are converted to nanotubes. J Clean Prod 297:126498. https://doi.org/10.1016/j.jclepro.2021.126498.
Olgun FAO, Kamer GM, Ozturk BD (2018) Synthesis of Fe3O4/Humic Acid/Silver nanoparticles and their application in Cu and Cd adsorption. Environ Res Technol 1:19–24.
Özkul SLÇ, Kaba İ, Olgun FAO (2024) Unravelling the potential of magnetic nanoparticles: a comprehensive review of design and applications in analytical chemistry. Anal Methods 16:3620–3640. https://doi.org/10.1039/d4ay00206g.
Padervand M, Ghasemi S, Hajiahmadi S et al. (2022) Multifunctional Ag/AgCl/ZnTiO3 structures as highly efficient photocatalysts for the removal of nitrophenols, CO2 photoreduction, biomedical waste treatment, and bacteria inactivation. Appl Catal a Gen 643:118794. https://doi.org/10.1016/j.apcata.2022.118794.
Padervand M, Heidarpour H, Goshadehzehn M, Hajiahmadi S (2020) Photocatalytic degradation of 3-methyl-4-nitrophenol over Ag/AgCl-decorated/[MOYI]-coated/ZnO nanostructures: Material characterization, photocatalytic performance, and in-vivo toxicity assessment of the photoproducts. Environ Technol Innov 21:101212. https://doi.org/10.1016/j.eti.2020.101212.
Padervand M, Nasiri F, Hajiahmadi S et al. (2022) Ag@Ag2MoO4 decorated polyoxomolybdate/C3N4 nanostructures as highly efficient photocatalysts for the wastewater treatment and cancer cells killing under visible light. Inorg Chem Commun 141:109500. https://doi.org/10.1016/j.inoche.2022.109500.
Pham P, Rashid M, Cai Y et al. (2020) Removal of As(III) from Water Using the Adsorptive and Photocatalytic Properties of Humic Acid-Coated Magnetite Nanoparticles. Nanomaterials 10:1604. https://doi.org/10.3390/nano10081604.
Qin W, Yang C, Yi R, Gao G (2010) Hydrothermal synthesis and characterization of Single-Crystalline -FE2O3Nanocubes. J Nanomater 2011:1–5. https://doi.org/10.1155/2011/159259.
Ribas LN, De Sousa Bulhões LO, Da Silva WL (2020) Study of the photocatalytic activity using silica-based materials doped with silver nanoparticles for degradation of rhodamine B dye. Water Air Soil Pollut 231:. https://doi.org/10.1007/s11270-020-04553-7.
Rosman R, Saifullah B, Maniam S et al. (2018) Improved anticancer effect of Magnetite nanocomposite formulation of GALLIC acid (FE3O4-PEG-GA) against lung, breast and colon cancer cells. Nanomaterials 8:83. https://doi.org/10.3390/nano8020083.
Sallam SA, El-Subruiti GM, Eltaweil AS (2018) Facile synthesis of AG–Γ-FE2O3 superior nanocomposite for catalytic reduction of nitroaromatic compounds and catalytic degradation of methyl orange. Catal Lett 148:3701–3714. https://doi.org/10.1007/s10562-018-2569-z.
Shan C, Su Z, Liu Z et al. (2023) One-Step synthesis of AG2O/FE3O4 magnetic photocatalyst for efficient organic pollutant removal via Wide-Spectral-Response Photocatalysis–Fenton Coupling. Molecules 28:4155. https://doi.org/10.3390/molecules28104155.
Shan R, Lu L, Gu J et al. (2020) Photocatalytic degradation of methyl orange by Ag/TiO2/biochar composite catalysts in aqueous solutions. Mater Sci Semiconductor Process 114:105088. https://doi.org/10.1016/j.mssp.2020.105088.
Sharma J, Sharma S, Soni V (2021) Classification and impact of synthetic textile dyes on Aquatic Flora: A review. Regional Stud Mar Sci 45:101802. https://doi.org/10.1016/j.rsma.2021.101802.
Sihem L, Hanine D, Faiza B (2020) Antibacterial activity of A-FE2O3 and A-FE2O3@AG nanoparticles prepared by Urtica leaf extract. Nanotechnologies Russ 15:198–203. https://doi.org/10.1134/s1995078020020135.
Solayman HM, Hossen MdA, Aziz AA et al. (2023) Performance evaluation of dye wastewater treatment technologies: A review. J Environ Chem Eng 11:109610. https://doi.org/10.1016/j.jece.2023.109610.
Tan KH, Shih YH, Chen WL (2024) Facile preparation of environmental benign LED white light active humic acid nanolayer coated titanium dioxide photocatalyst for bisphenol A degradation. Chemosphere 355:141710. https://doi.org/10.1016/j.chemosphere.2024.141710.
Tkaczyk A, Mitrowska K, Posyniak A (2020) Synthetic organic dyes as contaminants of the aquatic environment and their implications for ecosystems: A review. Sci Total Environ 717:137222. https://doi.org/10.1016/j.scitotenv.2020.137222.
Velegraki G, Vamvasakis I, Papadas IT et al. (2019) Boosting photochemical activity by Ni doping of mesoporous CoO nanoparticle assemblies. Inorg Chem Front 6:765–774. https://doi.org/10.1039/c8qi01324a.
Velusamy S, Roy A, Sundaram S, Mallick TK (2021) A review on heavy metal ions and containing dyes removal through Graphene Oxide-Based Adsorption Strategies for textile wastewater treatment. Chem Rec 21:1570–1610. https://doi.org/10.1002/tcr.202000153.

Wang C, Rong Z, Wang J et al. (2016) Seed-mediated synthesis of high-performance silver-coated magnetic nanoparticles and their use as effective SERS substrates. Colloids Surf a Physicochem Eng Asp 506:393–401. https://doi.org/10.1016/j.colsurfa.2016.05.103.

Wang H, Xie Z, Wang X, Jia Y (2020) NABIS2 as a novel indirect bandgap full spectrum photocatalyst: Synthesis and application. Catalysts 10:413. https://doi.org/10.3390/catal10040413.

Wu W, Shan G, Wang S et al. (2016) Environmentally relevant impacts of nano-TiO2 on abiotic degradation of bisphenol A under sunlight irradiation. Environ Pollut 216:166–172. https://doi.org/10.1016/j.envpol.2016.05.079.

Xu D, Zhang S-N, Chen J-S, Li X-H (2022) Design of the synergistic rectifying interfaces in Mott–Schottky Catalysts. Chem Rev 123:1–30. https://doi.org/10.1021/acs.chemrev.2c00426.

Xue S, Wang Y, Bo W et al. (2023) Calcium-doped magnetic humic acid nano particles for the efficient removal of heavy metals from wastewater: the role of Ca. Environ Technol 45:3228–3243. https://doi.org/10.1080/09593330.2023.2213832.

Yadav BS, Singh R, Vishwakarma AK, Kumar N (2020) Facile synthesis of substantially magnetic hollow nanospheres of maghemite (γ-Fe2O3) originated from magnetite (Fe3O4) via solvothermal method. J Superconductivity Nov Magn 33:2199–2208. https://doi.org/10.1007/s10948-020-05481-7.

Yang D-P, Gao F, Cui D-X, Yang M (2009) Microwave rapid synthesis of nanoporous FE3O4 magnetic microspheres. Curr Nanosci 5:485–488. https://doi.org/10.2174/157341309789378050.

Zhang J, Li X, Xu H et al. (2023) Coating magnetic nanoparticles with artificial humic acid derived from rice straw for effective removal of tetracycline antibiotics. Ind Crops Products 200:116781. https://doi.org/10.1016/j.indcrop.2023.116781.

Zhang X, Li M, Liu C et al. (2021) Enhanced the efficiency of photocatalytic degradation of methylene blue by construction of Z-Scheme G-C3N4/BIVO4 heterojunction. Coatings 11:1027. https://doi.org/10.3390/coatings11091027.